A Universal Ratio Snow Index for Fractional Snow Cover Estimation

Gongxue Wang, Lingmei Jiang, Jiancheng Shi, *Fellow, IEEE*, and Xu Su

Abstract—The moderate resolution imaging spectroradiometer (MODIS) snow algorithm has been used to generate global fractional snow cover (FSC) at a pixel size of 500 m using a linear regression relationship (called "FRA6T") between FSC and the normalized difference snow index (NDSI). However, the linear relationship is problematic because of the considerable NDSI variation in nonsnow conditions. In this letter, we propose a universal ratio snow index (URSI), which is the ratio of the visible reflectance and the sum of the near infrared and shortwave infrared reflectances. It is called "universal" because it has weak sensitivity under snow-free ground conditions and, therefore, can improve the stability of the linear snow index methodology. A comparison between NDSI and URSI with regard to estimate FSC using the linear snow index methodology is carried out for the Tibetan Plateau. The scatter plots of MODIS NDSI/URSI and Landsat-7 Enhanced Thematic Mapper Plus (ETM+) FSC indicate that a linear relationship can be assumed for both NDSI and URSI for barren land conditions and is more appropriate for URSI than it is for NDSI in forested areas. Validation efforts show that the linear relationship using URSI (designated "FracURSI") achieves fewer errors in FSC estimation compared with the developed NDSI method ("FracNDSI"), particularly for forested areas and for moderate FSC values. Averaged over all comparisons, the root-mean-square error (RMSE) of FSC estimates for FRA6T is 0.13, and for FracNDSI is 0.12, whereas FracURSI RMSE is 0.11.

Index Terms—Fractional snow cover (FSC), moderate resolution imaging spectroradiometer (MODIS), normalized difference snow index (NDSI), universal ratio snow index (URSI).

I. INTRODUCTION

SNOW cover plays an important and active role in the water cycle, surface radiation budget and climate change. Spring and early summer snowmelt occupies a significant proportion of the sources of midlatitude mountain runoff [1]. Snow's high albedo and low heat conductivity, along with its highly variable spatial extent, strongly influence the surface radiation budget. The retreat and advance of glaciers and perennial snow cover are sensitive to climate change.

The accurate estimation of the spatial distribution of snow cover can be pursued through optical remote sensing [2]–[8]. Snow-covered area from satellite imagery is generally estimated pixel by pixel through the determination of snow's presence/absence or, more precisely, the retrieval of snow's area fraction, i.e., fractional snow cover (FSC). The discrimination between snow/ice and other surface features is straightforward because of snow's unique spectral characteristics.

The reflectance of clean snow is very high at the visible wavelengths, falls drastically at the near-infrared wavelengths, and becomes very low at the shortwave infrared wavelengths. The normalized difference snow index (NDSI) proposed by Dozier [2] enlarges the snow's signal by taking the difference of visible and shortwave infrared reflectances divided by their sum. It is defined as follows:

$$\text{NDSI} = \frac{R_{\text{VIS}} - R_{\text{SWIR}}}{R_{\text{VIS}} + R_{\text{SWIR}}}. \qquad (1)$$

For decades, the criteria of using NDSI higher than a given threshold (generally 0.4) along with the screening of clouds and water bodies have been a fundamental approach in binary snow cover mapping [2], [7], [9]. NDSI is useful in FSC estimation as well [10]. Salomonson and Appel [11] established a linear statistical relationship (called "FRA6T" in the cited article) between Landsat-7 Enhanced Thematic Mapper Plus (ETM+) FSC and Terra Moderate Resolution Imaging Spectroradiometer (MODIS) NDSI using training data from Alaska, Siberia, and Labrador. FRA6T is presented as follows:

$$\text{FRA6T} = 1.45 \times \text{NDSI} - 0.01. \qquad (2)$$

We prefer the two-point form of the FRA6T (3) because it directly gives the NDSI thresholds determining snow-free and pure snow pixels, which are approximately 0 and 0.7, respectively

$$\text{FRA6T} = \frac{\text{NDSI} - 0.0069}{0.6950 - 0.0069}. \qquad (3)$$

The heterogeneity of land cover type can cause systematic errors in the snow-covered area estimation using the NDSI methodology. A main limitation of NDSI exists in forested areas, where the vegetation signal lowers NDSI for snow-covered pixels. Klein *et al.* [7] developed the snow-mapping (SNOMAP) method by using the NDSI versus the normalized difference vegetation index (NDVI) threshold field to classify snow-covered forest pixels. Even with this improvement, both the binary and FSC estimates of the MODIS standard snow cover product MOD10A1, using SNOMAP and FRA6T, respectively, have overestimates for land surfaces with a high vegetation fraction [12].

Gongxue Wang, Lingmei Jiang, and Xu Su are with the State Key Laboratory of Remote Sensing Science, Beijing Normal University, Beijing 100875, China, also with the Institute of Remote Sensing and Digital Earth, Chinese Academy of Sciences, Beijing 100010, China, and also with the Faculty of Geographical Science, Beijing Normal University, Beijing 100875, China (e-mail: wanggx@mail.bnu.edu.cn; jiang@bnu.edu.cn; suxu@mail.bnu.edu.cn).

Jiancheng Shi is with the State Key Laboratory of Remote Sensing Science, Jointly Sponsored by Beijing Normal University and Aerospace Information Research Institute of Chinese Academy of Sciences, Faculty of Geographical Science, Beijing Normal University, Beijing 100875, China (e-mail: shijc@radi.ac.cn).

Color versions of one or more of the figures in this letter are available online at http://ieeexplore.ieee.org.

Digital Object Identifier 10.1109/LGRS.2020.2982053

This article has been accepted for inclusion in a future issue of this journal. Content is final as presented, with the exception of pagination.

2   IEEE GEOSCIENCE AND REMOTE SENSING LETTERS

Band name	Landsat-7 ETM+		MODIS	
	Band number	Wavelength (μm)	Band number	Wavelength (μm)
Visible (green)	2	0.52-0.60	4	0.55-0.57
Near infrared	4	0.77-0.90	2	0.84-0.88
Shortwave infrared	5	1.55-1.75	6	1.63-1.65

There are other FSC estimation methods with more complexity than the snow spectral index method, including the multiple endmember spectral mixture analysis (MESMA) [5], [6], [13], SCAmod [14], and the artificial neural network (ANN) method [15]. MESMA is computationally expensive in the retrieval, and ANN requires complex design and training to establish its FSC algorithm. With representative model parameters, SCAmod can be feasible for forested areas. To take advantage of the simplicity of the snow spectral index methodology, it is necessary to reduce the uncertainties due to the heterogeneity of land cover type.

In this letter, we first propose a universal ratio snow index (URSI) as follows:

$$\text{URSI} = \frac{R_{\text{VIS}}}{R_{\text{NIR}} + R_{\text{SWIR}}}. \tag{4}$$

It is called "universal" because of its weak sensitivity to land cover type due to the incorporation of the near-infrared band. The specific bands of Landsat-7 ETM+ and MODIS are listed in Table I.

The purpose of this letter is to examine the rationality of the linear regression between Landsat-7 ETM+ FSC and Terra MODIS NDSI/URSI, with the land cover type factor taken into consideration. Moreover, we evaluate the performance and stability of FRA6T, the average FSC versus NDSI relationship, and the FSC versus URSI relationship derived from the linear regressions.

II. DATA

A. Satellite Data

The Landsat-7 ETM+ 30-m resolution surface reflectance is used to derive the FSC reference data, while the corresponding 500-m resolution surface reflectance from Terra MODIS (MOD09GA) is used to generate NDSI and URSI. Although there are available acquisitions from Landsat-5 Thematic Mapper (TM) and Landsat-8 Operational Land Imager (OLI), we employ Landsat-7 ETM+ instead of them to prevent the discrepancy in the viewing geometry condition. It is because Landsat-7 and Terra have simultaneous nadir overpasses, whereas Landsat-5 and Landsat-8 observations at midlatitudes are often at off-nadir views of Terra MODIS.

Nine Landsat-7 ETM+ scenes of the Tibetan Plateau with variation in solar zenith angle and land cover type are selected for the comparison between URSI and NDSI goodness-of-fit of the linear regressions with FSC and for the development of the FSC estimation algorithm. Six scenes are used for validation. These scenes are cloud-free or have very few clouds. The locations of these scenes are shown in Fig. 1, while the imaging conditions are listed in Table II.

B. Auxiliary Data

The terrain condition of the study area is represented by the 1 arc-second digital elevation model (DEM) from SRTM30 [16]. The spatial distribution of land cover type
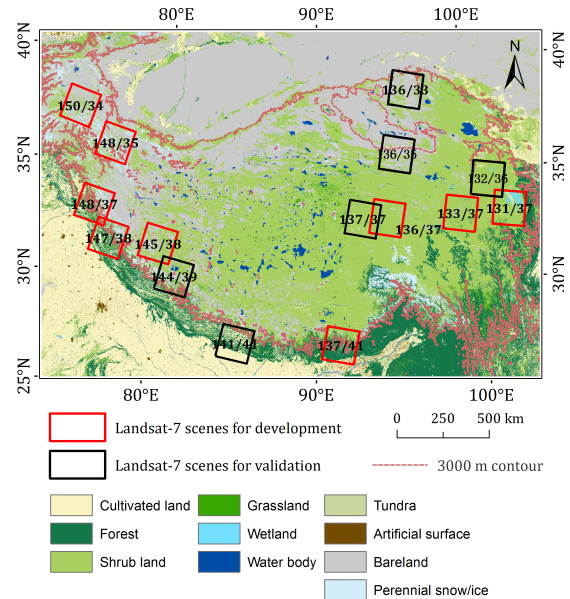

Fig. 1. Land cover of the study area and the locations of the Landsat-7 ETM+ image areas.

Scene (path/row)	Date (month/day/year)	Sun zenith (degree)	Sun azimuth (degree)	Land cover fraction of snow covered areas in each image (forest, grass and barren land)
Landsat-7 ETM+ images used in the comparison between NDSI and URSI for FSC estimation.				
148/037	03/21/02	41	138	19%, 29%, 51%
147/038	02/10/03	54	145	27%, 25%, 45%
137/041	01/03/03	57	150	27%, 66%, 7%
133/037	02/05/02	56	148	2%, 94%, 3%
131/037	11/22/02	57	156	6%, 92%, 0%
136/037	01/06/01	60	153	0%, 96%, 3%
150/034	06/04/02	25	121	0%, 22%, 77%
145/038	03/29/02	37	134	0%, 57%, 43%
148/035	03/21/03	43	141	0%, 21%, 79%
Landsat-7 ETM+ images used in the validation of the FSC estimation from NDSI and URSI. For scenes 144/039 and 141/041, we use the pixels with the land cover type of forest in the validation.				
144/039	03/06/02	45	139	26%, 40%, 33%
141/041	02/13//02	50	142	32%, 54%, 13%
132/036	11/26/01	59	157	0%, 99%, 1%
137/037	12/02/02	59	156	0%, 93%, 6%
136/035	10/24/02	51	154	0%, 43%, 56%
136/033	11/25/02	63	159	0%, 29%, 71%

is obtained from the GlobeLand30 data set [17]. Note that consider the areas with seasonal snow cover, the major forest type is coniferous forest on the Tibetan Plateau.

III. METHODOLOGY

A. Topographical Correction

The topographic effect is a nonnegligible limitation factor for snow cover mapping because midlatitude seasonal snow cover occurs extensively in mountainous areas. The relatively low sun height in winter can yield extensive terrain shadows, which can greatly weaken snow's signal. Moreover, shaded snow-free surfaces often have similar NDSI values to those of snow, and therefore, this issue creates a challenge for snow cover mapping using NDSI in rugged regions.

The topographic effect in the surface reflectance data of Landsat-7 ETM+ and Terra MODIS is eliminated using the C-correction method proposed by Teillet et al. [18]. The easily applicable C-correction is a semiempirical method. By incorporating the C factor, this correction method can

This article has been accepted for inclusion in a future issue of this journal. Content is final as presented, with the exception of pagination.

WANG *et al.*: URSI FOR FSC ESTIMATION

3

reduce overcorrection in low illumination areas caused by the simple cosine correction.

B. Generation of the Reference Data

As MESMA enables accurate and physically reasonable FSC retrieval, it has been used for Landsat data to generate reference FSC [5], [19]. Using the snow cover maps derived from 13 GaoFen-2 images at a spatial resolution of 3.2 m as a reference, Hao *et al.* [19] declared that the Landsat-8 OLI FSC based on MESMA can result in the overall accuracy of 0.946 and root-mean-square error (RMSE) of 0.094.

In this letter, the Landsat-7 ETM+ atmospherically and topographically corrected reflectance data from bands 1 through 5 and band 7 are used to derive the 30-m FSC based on the MESMA scheme proposed by Shi [13]. Snow, vegetation, and soil/rock endmembers are automatically extracted from concurrent images based on single-band reflectance and several spectral indices, including NDSI and NDVI. Typical endmembers are selected to make a parsimonious but representative endmember library of snow and nonsnow features [20].

The area fraction of snow (i.e., FSC) is calculated from

$$R_\lambda = \sum_{i=1}^{N} F_i R_{i,\lambda} + \varepsilon_\lambda \qquad (5)$$

where R_λ is the reflectance of a mixed pixel at wavelength λ, $R_{i,\lambda}$ is the reflectance of ith endmember of which the area fraction is F_i, and ε_λ is the residual error for the fit of the N endmembers.

The least-square method and the two-endmember (snow and nonsnow features) model are used to solve for FSC. The pixel-by-pixel FSC value is determined by an optimal solution that satisfies the spectral constraints and has the minimum RMSE.

It should be noted that radiometric saturation at the visible and near-infrared bands of Landsat-7 ETM+ often occurs for highly reflective surfaces, which are likely to be clean snow in the selected images. There seems no more preferable way to address this problem than to consider the saturated pixels as pure snow cover.

Finally, the reference FSC data are generated through the aggregation of Landsat-7 30-m FSC to match corresponding MODIS 500-m pixels except for the pixels identified as cloud or water bodies.

C. Linear Regression

Two different "models"/linear regressions were examined; namely, "model MA" expressed as FRA= a1 + b1*NDSI minimizing FRA deviations and "model MB" where NDSI = a2+b2*FRA minimizes NDSI deviations.

We use the "model MB" and the FSC range from 1% to 99% to perform the linear regressions between FSC and NDSI/URSI. FSC values of 0 are not used because some totally snow-free surfaces may have different characteristics from those surfaces neighboring or underneath snow cover. FSC values of 100% are excluded, as a large number of pixels clustered at 100% FSC with a variety of NDSI values tend to lower the performance of the linear regression.

A new criterion considering an FSC range of 10%–95% is additionally employed for "model MB" [11], which is referred to as "model New Criterion (NC)" in this letter. In fact, the relationship between FSC and NDSI for low FSC values differs from that for moderate and high FSC values in vegetated areas, which is discussed later in Section IV. Therefore, it is reasonable to examine the linear regressions using "model NC."
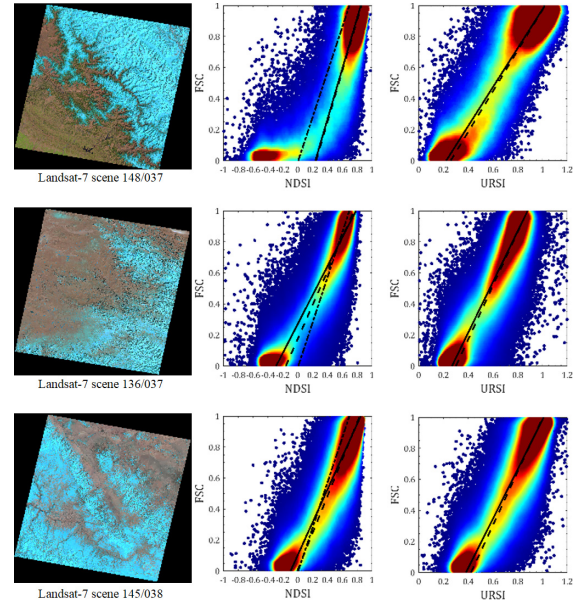

Fig. 2. Three Landsat-7 ETM+ images along with the scatter plots of Landsat-7 FSC versus the corresponding MODIS NDSI/URSI. The black solid line in the scatter plots indicates the linear regression using "model MB," the dashed line is the regression using "model NC", and the dashed-dotted line is the FRA6T relationship.

Three goodness-of-fit metrics, including mean absolute error (MAE), RMSE, and R-square (R^2), are employed to evaluate the linear regression relationships and the FSC estimation performance using the averaged relationships and the FRA6T approach.

IV. RESULTS

A. Comparison of the Linear Regressions

The linear regressions between FSC and NDSI and those between FSC and URSI are performed for the Landsat-7 ETM+ images listed in Table II. Fig. 2 illustrates three of these images for simplicity, which have numerous mixed pixels dominated by the land cover types of forest, grass-land, and barren ground, respectively.

In Landsat-7 ETM+ scene 148/037, acquired on 21 March 2002, URSI shows a major advantage over NDSI based on the linear relationship with FSC. Apparently, the relationship between FSC and NDSI for low FSC values differs greatly from that for moderate to high FSC values in forests. Similar evidence can be found in [10, Fig. 4(b)] and [11, Fig. 2(f)–(h)], as these two articles used Siberia as a study area. Therefore, the assumption of a linear relationship between FSC and NDSI can result in notable FSC errors.

In Landsat-7 ETM+ scene 136/037, acquired on 6 January 2001 and scene 145/038, acquired on 29 March 2002, URSI seems to perform similar to NDSI. The linear regressions using "model MB" with an FSC range of [1%, 99%] ("model MB") are similar to those using FSC values within [10%, 95%] ("model NC"), particularly for the use of URSI.

The "model MB" is more preferable for FSC versus URSI because low FSC values seem to have negligible impacts on URSI. The "model NC" may be suitable for FSC versus NDSI because the "model NC" results are more stable than those of the "model MB" throughout all of the scenes. Hence, we give the linear regression relationships and goodness-of-fit results in Table III only for NDSI with the "model NC" and for URSI with the "model MB."

TABLE III

COMPARISONS OF NDSI AND URSI FOR FSC ESTIMATION
USING LINEAR REGRESSION RELATIONSHIPS

Scene	Linear regression result (FSC vs NDSI and FSC vs URSI)		Goodness-of-fit (FSC vs NDSI and FSC vs URSI)		
	Snow-free threshold	Pure snow threshold	MAE	RMSE	R^2
148/037	0.25	0.86	0.12	0.18	0.66
	0.22	1.02	0.08	0.13	0.87
147/038	0.05	0.74	0.14	0.20	0.61
	0.20	0.93	0.11	0.16	0.83
137/041	0.19	0.74	0.16	0.22	0.52
	0.28	0.96	0.13	0.19	0.73
133/037	-0.28	0.75	0.15	0.20	0.52
	0.23	0.85	0.13	0.19	0.66
131/037	-0.18	0.85	0.14	0.18	0.56
	0.25	0.94	0.13	0.17	0.68
136/037	-0.16	0.76	0.11	0.15	0.70
	0.27	0.88	0.10	0.15	0.81
150/034	-0.16	0.87	0.15	0.21	0.55
	0.32	1.07	0.13	0.20	0.73
145/038	-0.01	0.83	0.12	0.17	0.65
	0.38	1.01	0.11	0.16	0.78
148/035	-0.08	0.84	0.12	0.16	0.69
	0.36	0.98	0.11	0.16	0.81
Average	-0.06	0.80			
	0.28	0.95			

A linear relationship between FSC and NDSI indicates that the FSC value for an observed NDSI is calculated from the linear interpolation between the snow-free and pure snow NDSI thresholds.

TABLE IV

VALIDATION RESULTS OF THE FSC ESTIMATION
USING FRA6T, FracNDSI, AND FracURSI

| Scene	Method	MAE	RMSE	R^2
144/039	FRA6T	0.07	0.15	0.91
	FracNDSI	0.06	0.13	0.92
	FracURSI	0.06	0.12	0.93
141/041	FRA6T	0.05	0.12	0.90
	FracNDSI	0.04	0.11	0.90
	FracURSI	0.04	0.10	0.92
132/036	FRA6T	0.07	0.15	0.65
	FracNDSI	0.07	0.14	0.67
	FracURSI	0.06	0.13	0.70
137/037	FRA6T	0.04	0.11	0.80
	FracNDSI	0.04	0.10	0.82
	FracURSI	0.04	0.10	0.83
136/035	FRA6T	0.07	0.13	0.89
	FracNDSI	0.06	0.11	0.90
	FracURSI	0.06	0.11	0.89
136/033	FRA6T	0.09	0.14	0.89
	FracNDSI	0.07	0.11	0.91
	FracURSI	0.08	0.12	0.89
Average	FRA6T	0.07	0.13	0.84
	FracNDSI	0.06	0.12	0.85
	FracURSI	0.06	0.11	0.86
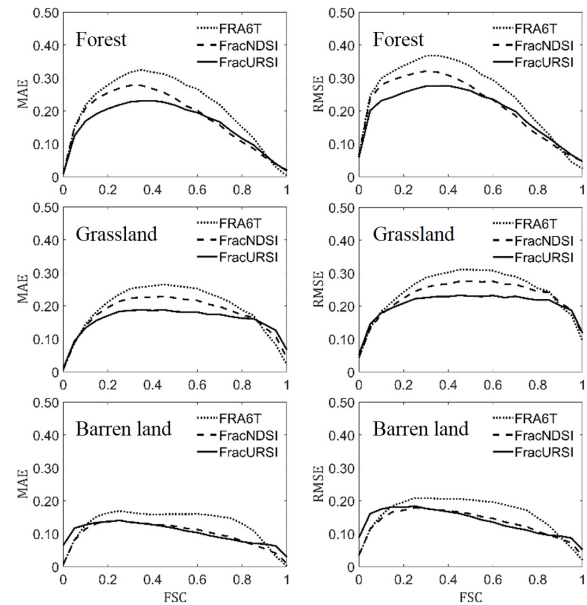
Fig. 3. Variability in MAE and RMSE according to the FSC estimates over various land surfaces using FRA6T, FracNDSI, and FracURSI.

In Table III, we present the linear regression relationships in the two-point form instead of the slope-intercept form. The two-point form clearly represents the NDSI/URSI thresholds of the snow-free ground and pure snow, between which the linear interpolation determines the FSC estimate.

The comparisons from these nine Landsat-7 ETM+ scenes indicate that the goodness-of-fit of the linear regression using URSI is comparable to that using NDSI for grassland and barren land on the Tibetan Plateau. In these unforested areas, the R^2 results of the linear regressions between URSI and FSC are better than the results using NDSI, while their MAE and RMSE values are very close. In areas with numerous mixed snow and forest pixels, URSI shows the best goodness-of-fit results and an obvious advantage over NDSI.

Throughout these scenes, the linear regressions using URSI remain relatively stable compared with those using NDSI. The snow-free thresholds determined by the FSC versus URSI models vary from 0.20 to 0.38, while the corresponding results from the FSC versus NDSI models have a wider range (from -0.28 to 0.25). For the thresholds of pure snow, the FSC versus URSI models show a higher variation than that of the FSC versus NDSI models and thus may cause slight inaccuracies for high FSC values.

Table III also provides the averaged results of the FSC versus NDSI models and the FSC versus URSI models. Hereafter, the resulting linear relationships are referred to as "FracNDSI" and "FracURSI"

$$\text{FracNDSI} = 1.17 \times \text{NDSI} + 0.07 \quad (6)$$
$$\text{FracURSI} = 1.48 \times \text{URSI} - 0.41. \quad (7)$$

B. Validation

To examine the performance of FRA6T, FracNDSI, and FracURSI, we acquire six Landsat-7 ETM+ scenes and corresponding MODIS observations and then compare FSC estimates from the MODIS images using these three approaches with the reference data from Landsat-7 ETM+. The results are listed in Table IV.

As expected, FRA6T results in the worst FSC estimation for all of the scenes mainly because the training data of FRA6T from Alaska, Siberia, and Labrador poorly represent the ground conditions of the Tibetan Plateau. Notably, the MAE, RMSE, and R^2 values for FracNDSI and FracURSI are very close. Considering the effect of land cover type, we analyze the variation in MAE and RMSE of the three FSC estimation methods in Fig. 3. For forested ground and grassland, FracURSI has more plausible results than those of FracNDSI at a moderate FSC level, while they have very similar performance for other FSC values. However, FracURSI has errors a bit higher than those of FracNDSI for low FSC of barren ground. This is likely because, in the URSI, there is less of a difference between snow and barren land than

there is in the NDSI; hence, FracURSI results in some areas erroneously classified as snow. Low FSC estimates are found to be uncertain for the MODIS Snow Covered Area and Grain Size (MODSCAG) product and FRA6T as well. Therefore, MODSCAG reports FSC for the range from 0.15 to 1.0 [5], while MOD10A1 and MYD10A1 in Collection six reverse snow detections with NDSI < 0.10 (i.e., FSC < 0.135) to nonsnow [3]. For the use of URSI to estimate FSC, the FSC threshold of 0.15 is also recommended to alleviate spurious snow detections, especially in barren areas.

C. Limitation

As spectral reflectance is inherently nonnegative, NDSI falls within the range of [−1, +1], whereas the theoretical range of URSI is from 0 to ∞. Pure snow's URSI is roughly in the range of 0.8 to 1.2, while water's URSI is generally much higher. This indicates that URSI can be useful for separating water bodies from snow cover. In addition, URSI is less sensitive to noise than the straightforward ratio snow index (the reflectance ratio between the visible band and the shortwave infrared band) due to an additional near-infrared band used in the denominator.

V. Conclusion

The well-known MODIS snow cover product (the MOD10 suite) employs a linear snow index methodology to derive snow-covered areas. The linear relationship between NDSI and FSC assumed by this product is problematic to some extent considering the variation in land cover condition and has considerable errors in snow-covered forests where in fact NDSI behaves quite nonlinearly with FSC. The explanation of this nonlinearity is that the reflectance difference between snow and vegetation at the visible wavelengths differs greatly from that at the shortwave infrared. The drastic disparity breaks the approximate linearity between the single-band reflectance and FSC.

Here, we define a URSIas the visible band reflectance divided by the sum of the near-infrared and shortwave infrared reflectances. We incorporate the near infrared band because the reflectance difference between snow and vegetation differs slightly between the near-infrared and the shortwave infrared wavelengths. Moreover, the resulting URSI also has a tighter range for a variety of snow-free ground conditions than that of NDSI. This feature of URSI makes it "universal" due to its weak sensitivity to land cover types; therefore, it can improve the stability of the linear snow index methodology and its reasonability for continental-scale applications.

We compare NDSI and URSI in terms of the goodness-of-fit of linear regressions with FSC. The reference (approximate ground truth) data used in the comparisons is Landsat-7 ETM+ 30-m FSC derived from the MESMA of atmospherically and topographically corrected reflectance data. The corresponding NDSI and URSI are calculated using Terra MODIS 500-m observations. The results of the testing areas based on the Landsat-7 scenes indicate that URSI has better linear regression relationships than NDSI with FSC in forests and that the relationships are more stable as well.

Independent validations have been conducted for the averaged relationships between FSC and NDSI/URSI. Results show that the URSI method has fewer errors than the NDSI method for moderate FSC values in vegetated areas including forests and grassland, but slightly more errors for low FSC values under barren ground conditions. It is mainly because the URSI method sometimes has overestimation results for sandy and saline-alkali soil surfaces. A practical approach to reduce snow commission errors is to reclassify the "snow" pixels with FSC < 0.15 as snow-free.

References

[1] H. Wulf, B. Bookhagen, and D. Scherler, "Differentiating between rain, snow, and glacier contributions to river discharge in the western himalaya using remote-sensing data and distributed hydrological modeling," *Adv. Water Resour.*, vol. 88, pp. 152–169, Feb. 2016.

[2] J. Dozier, "Spectral signature of alpine snow cover from the landsat thematic mapper," *Remote Sens. Environ.*, vol. 28, pp. 9–22, Apr. 1989.

[3] G. A. Riggs, D. K. Hall, and M. O. Román, "MODIS snow products collection 6 user guide," Tech. Rep., Aug. 2016, pp. 1–66. [Online]. Available: https://modis-snow-ice.gsfc.nasa.gov/uploads/C6_MODIS_Snow_User_Guide.pdf

[4] A. W. Nolin, "Recent advances in remote sensing of seasonal snow," *J. Glaciol.*, vol. 56, no. 200, pp. 1141–1150, 2010.

[5] T. H. Painter, K. Rittger, C. McKenzie, P. Slaughter, R. E. Davis, and J. Dozier, "Retrieval of subpixel snow covered area, grain size, and albedo from MODIS," *Remote Sens. Environ.*, vol. 113, no. 4, pp. 868–879, Apr. 2009.

[6] P. Sirguey, R. Mathieu, and Y. Arnaud, "Subpixel monitoring of the seasonal snow cover with MODIS at 250 m spatial resolution in the Southern Alps of New Zealand: Methodology and accuracy assessment," *Remote Sens. Environ.*, vol. 113, no. 1, pp. 160–181, Jan. 2009.

[7] A. G. Klein, D. K. Hall, and G. A. Riggs, "Improving snow cover mapping in forests through the use of a canopy reflectance model," *Hydrol. Processes*, vol. 12, nos. 10–11, pp. 1723–1744, Aug. 1998.

[8] A. Frei *et al.*, "A review of global satellite-derived snow products," *Adv. Space Res.*, vol. 50, no. 8, pp. 1007–1029, Oct. 2012.

[9] H. Zhang *et al.*, "Ground-based evaluation of MODIS snow cover product v6 across China: Implications for the selection of NDSI threshold," *Sci. Total Environ.*, vol. 651, pp. 2712–2726, Feb. 2019.

[10] V. V. Salomonson and I. Appel, "Estimating fractional snow cover from MODIS using the normalized difference snow index," *Remote Sens. Environ.*, vol. 89, no. 3, pp. 351–360, Feb. 2004.

[11] V. V. Salomonson and I. Appel, "Development of the Aqua MODIS NDSI fractional snow cover algorithm and validation results," *IEEE Trans. Geosci. Remote Sens.*, vol. 44, no. 7, pp. 1747–1756, Jul. 2006.

[12] K. Rittger, T. H. Painter, and J. Dozier, "Assessment of methods for mapping snow cover from MODIS," *Adv. Water Resour.*, vol. 51, pp. 367–380, Jan. 2013.

[13] J. Shi, "An automatic algorithm on estimating sub-pixel snow cover from MODIS," *Quaternary Sci.*, vol. 32, no. 1, pp. 6–15, Jan. 2012.

[14] S. Metsämäki *et al.*, "Introduction to GlobSnow snow extent products with considerations for accuracy assessment," *Remote Sens. Environ.*, vol. 156, pp. 96–108, Jan. 2015.

[15] E. H. Czyzowska-Wisniewski, W. J. D. van Leeuwen, K. K. Hirschboeck, S. E. Marsh, and W. T. Wisniewski, "Fractional snow cover estimation in complex alpine-forested environments using an artificial neural network," *Remote Sens. Environ.*, vol. 156, pp. 403–417, Jan. 2015.

[16] T. G. Farr and M. Kobrick, "Shuttle radar topography mission produces a wealth of data," *EOS, Trans. Amer. Geophys. Union*, vol. 81, no. 48, pp. 583–585, 2000.

[17] J. Chen *et al.*, "Global land cover mapping at 30m resolution: A POK-based operational approach," *ISPRS J. Photogramm. Remote Sens.*, vol. 103, pp. 7–27, May 2015.

[18] P. M. Teillet, B. Guindon, and D. G. Goodenough, "On the slope-aspect correction of multispectral scanner data," *Can. J. Remote Sens.*, vol. 8, no. 2, pp. 84–106, Dec. 1982.

[19] S. Hao, L. Jiang, J. Shi, G. Wang, and X. Liu, "Assessment of MODIS-based fractional snow cover products over the tibetan plateau," *IEEE J. Sel. Topics Appl. Earth Observat., Remote Sens.*, vol. 12, no. 2, pp. 533–548, Feb. 2019.

[20] Y. Xu, J. Shi, and J. Du, "An improved endmember selection method based on vector length for MODIS reflectance channels," *Remote Sens.*, vol. 7, no. 5, pp. 6280–6295, May 2015.